Mitochondrial type-I prohibitins of *Arabidopsis thaliana* are required for supporting proficient meristem development

Olivier Van Aken[1,2], Tamara Pečenková[1,2,†], Brigitte van de Cotte[1,2], Riet De Rycke[1,2], Dominique Eeckhout[1,2], Hillel Fromm[3], Geert De Jaeger[1,2], Erwin Witters[4], Gerrit T. S. Beemster[1,2], Dirk Inzé[1,2] and Frank Van Breusegem[1,2,*]

[1]*Department of Plant Systems Biology, Flanders Institute for Biotechnology, 9052 Gent, Belgium,*
[2]*Department of Molecular Genetics, Ghent University, 9052 Gent, Belgium,*
[3]*Department of Plant Sciences, Tel Aviv University, Tel Aviv 69978, Israel, and*
[4]*Centre for Proteome Analysis and Mass Spectrometry, University of Antwerp, 2020 Antwerpen, Belgium*

Summary

The *Arabidopsis thaliana* genome expresses five evolutionarily conserved prohibitin (PHB) genes that are divided into type-I (*AtPHB3* and *AtPHB4*) and type-II (*AtPHB1*, *AtPHB2* and *AtPHB6*) classes, based on their phylogenetic relationships with yeast PHB1 and PHB2, respectively. Yeast and animal PHBs are reported to have diverse roles in the cell cycle, mitochondrial electron transport, aging and apoptosis. All transcribed Arabidopsis *PHB* genes are primarily expressed in both shoot and root proliferative tissues, where they are present in mitochondrial multimeric complexes. Loss of function of the type-I *AtPHB4* had no phenotypic effects, while loss of function of the homologous *AtPHB3* caused mitochondrial swelling, decreased meristematic cell production, increased cell division time and reduced cell expansion rates, leading to severe growth retardation. Double knockout *atphb3 atphb4* plants were not viable, but transgenic lines over-expressing *AtPHB3* or *AtPHB4* showed leaf shape aberrations and an increased shoot branching phenotype. Genome-wide microarray analysis revealed that both knockout and overexpression perturbations of *AtPHB3* and *AtPHB4* provoked an altered abundance of mitochondrial and stress-related transcripts. We propose that plant type-I PHBs take part in protein complexes that are necessary for proficient mitochondrial function or biogenesis, thereby supporting cell division and differentiation in apical tissues.

Keywords: Arabidopsis, prohibitins, mitochondria, development, cell division.

Introduction

Prohibitins (PHBs) were originally discovered as tumor-suppressor genes in mammalian cells (McClung *et al.*, 1989). The human *PHB* gene is located on the 17q21 locus together with *Breast Cancer 1* (*BRCA1*). The medical importance of targeting PHBs in various disease states has recently been reviewed (Mishra *et al.*, 2005). Prohibitins are evolutionarily conserved proteins and have been reported in various cellular processes, such as signaling (Rajalingam *et al.*, 2005), cell cycle regulation (Gamble *et al.*, 2004; Wang *et al.*, 2002), mitochondrial respiration (Coates *et al.*, 2001; Nijtmans *et al.*, 2000), cell death (Fusaro *et al.*, 2003) and aging (Coates *et al.*, 1997). This apparent functional diversity is also reflected in an ongoing debate about the subcellular location of PHBs because they have been reported as plasma membrane, nuclear and mitochondrial proteins. In mammals, their plasma membrane location has been inferred from protein–protein interactions with plasma membrane receptors, such as the IgM antigen receptor (Rajalingam *et al.*, 2005; Terashima *et al.*, 1994). A nuclear role for mammalian PHBs as negative cell cycle regulators is deduced from binding and repression of the E2F transcriptional cell cycle activator through recruitment of co-repressors, such as histone deacetylase 1, to E2F-responsive promoters, and is further supported by immunolocalization studies (Fusaro *et al.*, 2003; Wang *et al.*, 2002). However, other observations demonstrate a mitochondrial location and function (Coates *et al.*, 1997; Ikonen *et al.*, 1995). Yeast and animal PHB1 and PHB2 localize in the mitochondrial inner membrane, are

interdependent for their stability (Coates *et al.*, 1997, 2001; Nijtmans *et al.*, 2000) and appear as heterodimers in multimeric complexes of 1–2 MDa with a ring-shaped structure (Nijtmans *et al.*, 2000; Artal-Sanz *et al.*, 2003; Tatsuta *et al.*, 2005). The yeast PHB complex interacts with the mitochondrial matrix-ATPases associated with a variety of activities (m-AAA proteases; Steglich *et al.*, 1999) and protects *de novo* synthesized mitochondrially encoded proteins against degradation by the m-AAA protease. Therefore, PHBs are proposed to act as chaperones in mitochondrial respiratory chain assembly. In plants, subcellular fractionations indicated a mitochondrial enrichment (Snedden and Fromm, 1997) and a proteome analysis of purified *Arabidopsis thaliana* mitochondria identified PHBs as integral mitochondrial membrane proteins (Millar *et al.*, 2001).

The importance of the PHB complex was first demonstrated in yeast, because double knockouts of *PHB1* and *PHB2* were viable but suffered from a severe loss of mitochondrial membrane potential together with a reduced replicative lifespan (Coates *et al.*, 1997). Depletion of *PHB1* and/or *PHB2* mRNA by RNA-mediated interference in *Caenorhabditis elegans* resulted in arrest of embryonic development (Artal-Sanz *et al.*, 2003) and virus-induced gene silencing of PHBs in *Petunia hybrida* caused abnormal leaf morphology, with fewer, but larger, cells and accelerated senescence (Chen *et al.*, 2005). Recently, a role for PHBs in mitochondrial biogenesis has been suggested in *Nicotiana benthamiana* (Ahn *et al.*, 2006). We demonstrate that Arabidopsis PHBs (AtPHBs) are mitochondrial factors that are predominantly expressed in proliferative tissues and provide genetic evidence that type-I plant PHBs are necessary to support cell division in apical tissues.

Results

Arabidopsis PHBs are targeted to the mitochondria

Prohibitins are strongly conserved across different taxa (Nijtmans *et al.*, 2000). A phylogenetic analysis revealed that the PHB protein family is split into two major groups that we designated type-I and type-II, with respect to their homology with yeast PHB1 and PHB2 (Figure 1a). All analyzed organisms contain at least one member of both types, suggesting that type-I and type-II PHBs are functionally interdependent. Generally, type-I PHBs are smaller than their type-II counterparts in the same species and have more acidic pI values. The Arabidopsis genome contains three type-I and four type-II *PHB* genes, which probably originate from ancestral duplications, as suggested by their conserved intron/exon composition: type-I and type-II *AtPHB* genes have one and four introns, respectively (Figure 1b). Phylogenetically, AtPHB5 and AtPHB7 are more divergent and are outliers in the set of plant PHBs. As no expressed sequence tags have been identified for both genes they are probably pseudo-genes or only expressed at very low levels under unidentified specific conditions.

No canonical mitochondrial transit peptide or nuclear localization signals were detected in the AtPHB protein sequences, although the prediction tool TMHMM2 suggested a putative N-terminal transmembrane helix between the 6th and 40th amino acid (Krogh *et al.*, 2001). To experimentally assess the function of this N-terminal domain in the subcellular targeting of AtPHBs, for all seven *AtPHB* genes we produced transgenic Arabidopsis plants containing the respective *AtPHB* promoter, the first *AtPHB* exon translationally fused to a green fluorescent protein (GFP)-β-glucuronidase (GUS) reporter cassette. The first *AtPHB* exons were expected to contain the putative targeting domains. The GUS histochemical stainings on the ProAtPHB:GFP–GUS lines revealed that the *AtPHB* promoters drive expression predominantly in proliferative tissues (see below), except for *AtPHB5* and *AtPHB7* in which no expression was visible. At the subcellular level, the fluorescent signal was observed in a punctate pattern (Figure 1c). Co-localization experiments with the Mitotracker mitochondrial marker demonstrated that this pattern matched that of the mitochondria for all five AtPHB:GFP–GUS fusion proteins (Figure 1c). The full-length open reading frames (ORFs) of AtPHBs were amplified by PCR, translationally fused upstream and downstream of a GFP-coding sequence and stably transformed into tobacco (*Nicotiana tabacum*) Bright Yellow-2 suspension cells. The corresponding cDNAs for *AtPHB5* and *AtPHB7* could not be cloned. For the GFP–AtPHB fusion constructs, the GFP signal was diffused throughout the cytoplasm, but for the C-terminal AtPHB–GFP fusions, it clearly matched the Mitotracker marker (Figure 1d,e). Taken together, these results indicate that AtPHBs are targeted to the mitochondria by an N-terminal peptide.

AtPHBs form a multimeric protein complex

In both yeast and animal mitochondria, PHBs have previously been demonstrated to form complexes of 1–2 MDa that possibly function as chaperones for components of the respiration chain (Nijtmans *et al.*, 2000; Steglich *et al.*, 1999). To assess whether AtPHBs are also part of a multimeric complex, we identified the interacting proteins within such a complex with a tandem affinity purification (TAP)/mass spectrometry (MS)-based approach (Rigaut *et al.*, 1999; Van Leene *et al.*, 2007). Arabidopsis cell suspension cultures were stably transformed by *Agrobacterium tumefaciens*-mediated co-cultivation with a Pro35S:AtPHB3-TAP cassette. The TAP tag consisted of two IgG-binding domains of the *Staphylococcus aureus* protein A (ZZ) and a calmodulin-binding peptide (CBP), separated by a tobacco etch virus (TEV) protease cleavage site. Based on the presence of the double tag, two-step affinity purification was performed. In two independent experiments with AtPHB3 as bait,
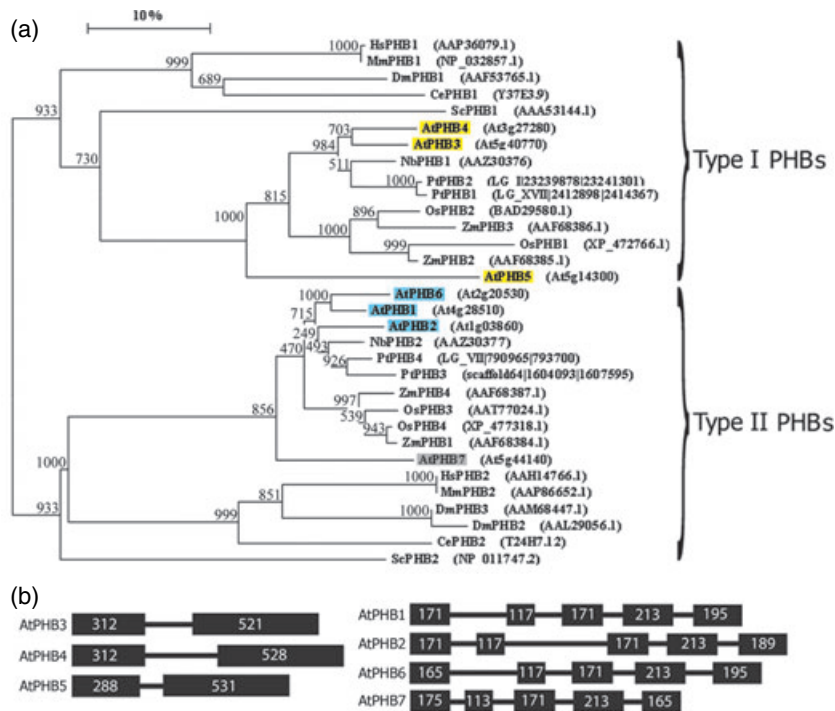
(a)

(b)

(c)

AtPHB4:GFP-GUS   Mitotracker   Overlay

(d)

GFP-AtPHB4   Mitotracker   Overlay

(e)

AtPHB4-GFP   Mitotracker   Overlay

Figure 1. Phylogenetic analysis and mitochondrial targeting of the prohibitin (PHB) protein family.
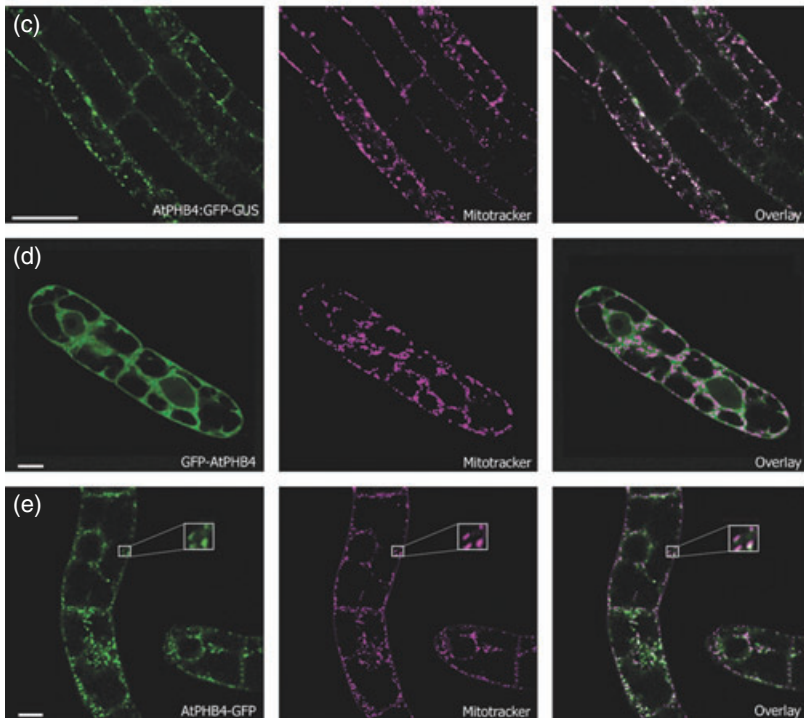
(a) Phylogenetic clustering of the PHB homologs from different phylogenetic taxa (At, *Arabidopsis thaliana*; Ce, *Caenorhabditis elegans*; Dm, *Drosophila melanogaster*; Hs, *Homo sapiens*; Mm, *Mus musculus*; Nb, *Nicotiana benthamiana*; Os, *Oryza sativa*; Pt, *Populus trichocarpa*; Sc, *Saccharomyces cerevisiae*; Zm, *Zea mays*). The scale bar represents 10% sequence divergence and the numbers at each node indicate bootstrap values. Arabidopsis type-I and type-II AtPHBs are indicated in yellow and blue, respectively.

(b) Exon/intron structure of the seven *AtPHB* genes. For each exon, the length in base pairs is indicated.

(c) Translational fusion of the first *AtPHB4* exon, intron and part of the second exon with GFP-GUS, under control of the *AtPHB4* promoter, co-localization with the mitochondrial marker Mito-tracker and overlay in root cortical cells.

(d) N-terminal GFP fusion with *AtPHB4* in tobacco BY-2 cell suspension.

(e) C-terminal GFP fusion with *AtPHB4* in tobacco BY-2 cell suspension. Insets are a 2.5× magnification of the indicated region. Scale bars = 50 μm (c), 10 μm (d,e).

AtPHB4 and the type-II AtPHB1, AtPHB2 and AtPHB6 were isolated (Table 1). In addition AtPHB3 occurred in the tagged and untagged form, indicating that it can directly or indirectly bind itself. The AtPHBs were detected at their predicted molecular mass and peptides were found close to the N-termini, suggesting that, as in other organisms, no leader peptide is cleaved during import of AtPHB into the mitochondria (Artal-Sanz *et al.*, 2003). The other proteins included the mitochondrial isocitrate dehydrogenase IDH1, a phosphoglycerate kinase, a DEAD box RNA helicase and three expressed proteins (Table 1). From these *in vivo* interaction experiments, we can conclude that all expressed AtPHBs are present within a multimeric complex.

Table 1 *In vivo* interaction partners of AtPHB3 as determined by tandem affinity purification

AGI code	Description	MW (kDa)	Peptide count	Protein score	Best ion score	Mitochondrial location
At5g40770	AtPHB3	30.4	13	536	159	Yes
At4g28510	AtPHB1	31.7	11	279	124	Yes
At1g03860	AtPHB2	31.8	7	274	124	Yes
At2g20530	AtPHB6	31.6	7	262	124	Yes
At3g27280	AtPHB4	30.6	8	182	81	Yes
At1g79550	Phosphoglycerate kinase	42.1	9	163	52	Associated with
At3g58510	DEAD box RNA helicase	66.0	18	144		
At1g70220	Expressed protein	18.9	6	86		
At4g35260	Isocitrate dehydrogenase IDH1	39.6	4	67	39	Yes
At2g38823	Expressed protein	31.0	3	55	35	
At5g20090	Expressed protein	12.4	1	41	32	Yes

AtPHB genes are predominantly expressed in proliferating tissues

To obtain an initial insight into the *AtPHB* expression characteristics, we surveyed publicly available expression data accessible through the Genevestigator toolbox (Zimmermann *et al.*, 2004). The highest *AtPHB* transcript levels were found particularly in proliferative tissues, such as the shoot apex, the root tip, young leaves and cell suspensions (Figure 2a). Tissue-specific expression was further explored by GUS histochemical staining on transgenic plants containing the promoter *PHB:GFP–GUS* fusion constructs in which the first *AtPHB* exon, intron and part of the second exon were translationally fused to GFP–GUS. Very similar results were obtained with all *AtPHB* promoter constructs, with the exception of *AtPHB5* and *AtPHB7*, for which no staining was observed. We describe the results for *AtPHB4* that are representative for all five expressed *AtPHB* promoters.

Sometimes GUS staining was observed in vasculature, but was most prominent in both shoot and root apical tissues (Figure 2b,e,f). Longitudinal sections through the shoot apex of young seedlings revealed strong staining in the young leaf primordia (Figure 2c). In cotyledons, hypocotyls and differentiating rosette leaves, *AtPHB* promoter activity was also detectable in stomatal meristemoid cells, guard mother cells and trichomes (Figure 2d,f). In mature leaves GUS staining was hardly detectable (Figure 2e). In inflorescences, the *AtPHB4* promoter was also primarily active in the apical region, young leaves, emerging axillary buds and young flowers (Figure 2g). Within the anthers, GUS staining was located in the proximity of the sporogenous tissue and disappeared shortly after maturation (Figure 2h). In immature seeds, globular embryos, though not the suspensor cells, were significantly stained (Figure 2i).

In roots, the *AtPHB4* promoter was predominantly active in the meristematic zone. The expression diminished in the elongation zone and did not exceed background levels in the differentiation zone (Figure 2j). In cross-sections through the meristematic zone, the expression levels were lower in protophloem cells than in surrounding tissues (Figure 2k).

No promoter activity was observed in root cap cells. In the elongation zone, expression was highest in epidermal cells, particularly in the trichoblasts (data not shown). The *AtPHB4* promoter was also highly active in developing adventive and lateral root meristems (Figures 2b,l and 3a).

Lateral root initiation is induced by auxin-mediated cell cycle activation (Himanen *et al.*, 2002). To assess the auxin responsiveness of *AtPHB* expression, ProAtPHB:GFP–GUS seeds were germinated on medium containing the auxin transport inhibitor naphthylphthalamic acid (NPA). No lateral root initials were formed and no clear staining was discernible in root pericycle cells 72 h after germination. Six hours after transfer to medium containing the auxin naphthaleneacetic acid (NAA), elevated expression was observed in pericycle cells at the protoxylem poles (Figure 3c,d), indicating that the *AtPHB* promoter is already active during the first asymmetrical cell divisions of lateral root initiation. This auxin-inducible promoter activity is in line with increased *AtPHB* transcript abundance in a microarray analysis, in which *AtPHB1*, *AtPHB3* and *AtPHB4* transcripts accumulated within 6 h of the application of auxin (Vanneste *et al.*, 2005; Figure 3b).

The abundance of *AtPHB* transcript was also monitored by real-time reverse transcriptase (RT)-PCR in a leaf development time series (Beemster *et al.*, 2005; Figure 3e). Transcript levels of all expressed *AtPHB* genes were highest in proliferating leaf tissue (days 8–12), decreased during the expansion phase (days 12–19) and reached minimal levels in mature leaf tissue (days 19–24). This observation is consistent with the ProAtPHB histochemical staining patterns (Figure 2h,i), in which expression was highest in the youngest leaves and faded toward leaf maturity. Thus, *AtPHB* genes are primarily expressed in proliferative tissues and dividing cells.

Loss of function of AtPHB3 provokes developmental phenotypes

A loss-of-function mutant *atphb3*^{KO} (SALK_020707) contained a T-DNA insertion at the end of exon 1 (Figure 4a).
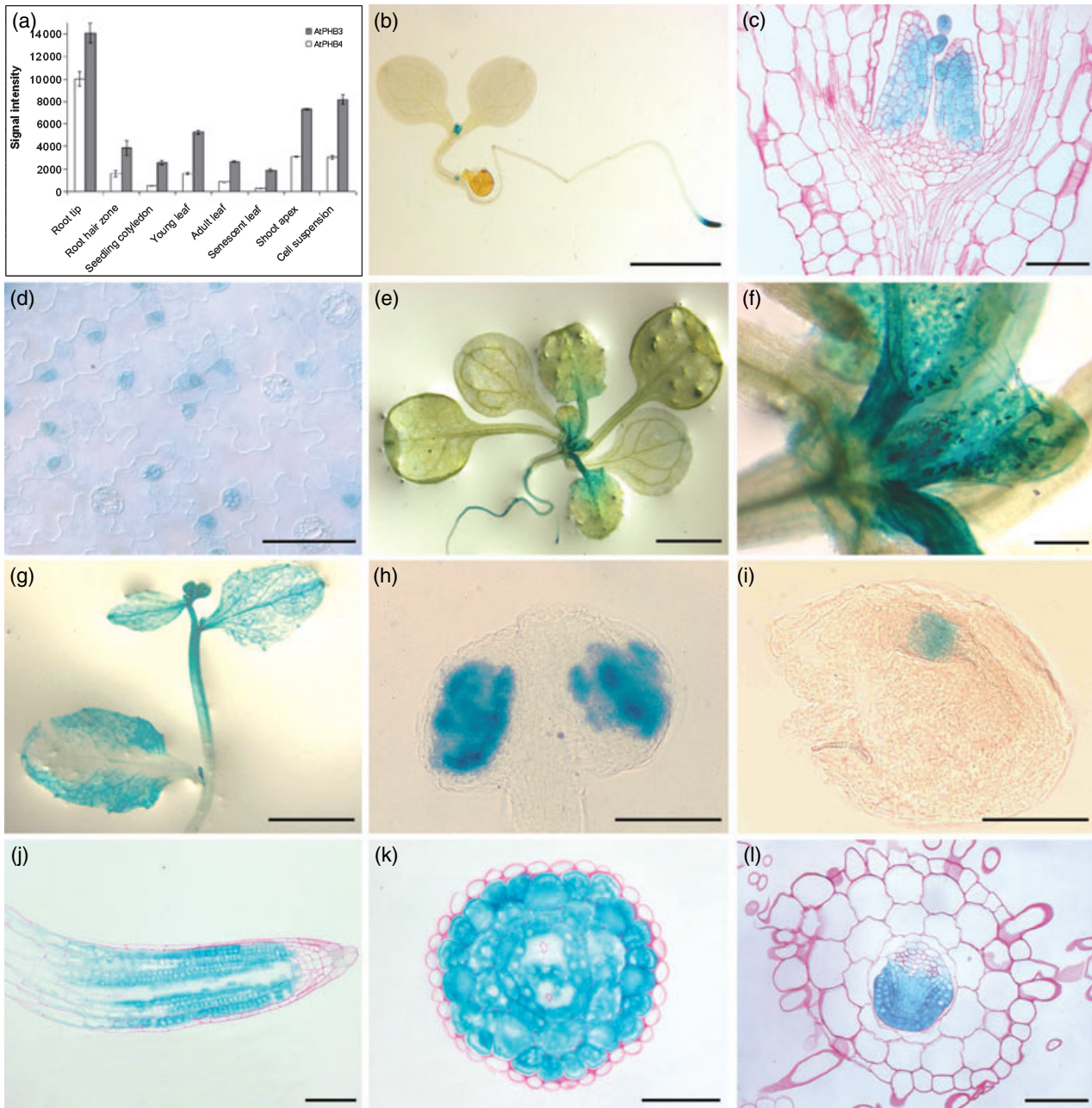
Figure 2. Expression analysis and histochemical GUS stainings of promoter-*AtPHB4*:GFP-GUS reporter lines.
(a) Average signal intensities of the *AtPHB4* probe in microarray experiments on specific Arabidopsis tissues, as collected from Genevestigator.
(b) GUS staining on a 3-day-old seedling.
(c) Longitudinal section through the apical meristem.
(d) Differential interference contrast image of cotyledon epidermis.
(e) Seedling at developmental stage 1.6.
(f) Close-up of (e).
(g) Inflorescence apex.
(h) Immature anther from a developing flower.
(i) Immature seed from a developing silique.
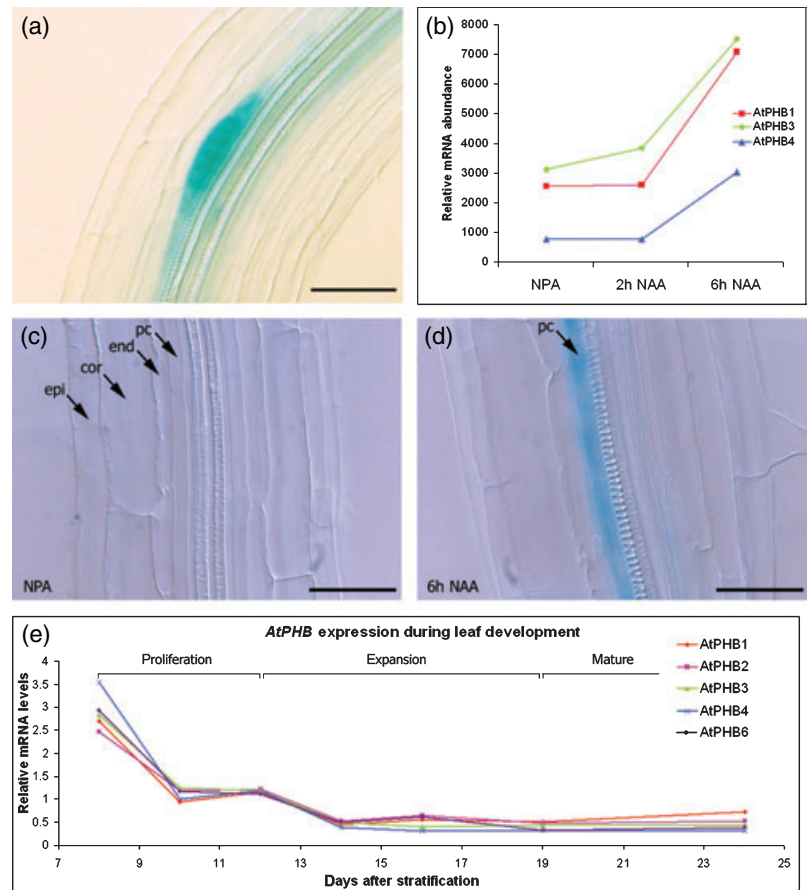(j) Longitudinal section through the root apical meristem.
(k) Transverse section through the root apical meristem.
(l) Transverse section through the adventive root meristem.
Bars = 50 μm (c,d,h,i,k,l), 100 μm (j), 200 μm (f), 2 mm (b,e), 3 mm (g).

Figure 3. *AtPHB* expression in lateral root initiation and leaf development.
(a) Differential interference contrast image of a lateral root primordium.
(b) Relative expression values of *AtPHB1*, *At-PHB3* and *AtPHB4* 2 h and 6 h after transfer from naphthylphthalamic acid (NPA) to naphthaleneacetic acid (NAA) (Vanneste *et al.*, 2005).
(c) GUS staining on the root of a 3-day-old seedling germinated on the auxin transport inhibitor NPA.
(d) GUS staining on the root of a 3-day-old seedling 6 h after transfer from NPA to NAA.
(e) *AtPHB* mRNA levels during development of leaf 1 and 2 as determined by real-time RT-PCR.
cor, cortex; end, endodermis; epi, epidermis; pc, pericycle. Bar = 50 μm.

RNA gel blot analysis showed that, in homozygous *atphb3^KO* plants, the 1.2-kb sized *AtPHB3* transcript levels were strongly reduced, but that a transcript of approximately 2 kb accumulated (Figure 4b). The *atphb3^KO* plants had obvious developmental phenotypes with severe growth retardation throughout their development. Germination of *atphb3^KO* seeds was delayed by 1–2 days compared with wild-type and *atphb4^KO* plants (Supplementary Figure S1). The *Atphb3^KO* plants were severely retarded in growth throughout their development. Sections through the shoot apex of 3-day-old seedlings showed a significant delay in the development of leaf structures (Figure 4c). After 4 weeks of growth, the rosette of *atphb3^KO* plants had a leaf area that was more than 2.5-fold smaller than that of wild-type plants and had developed fewer leaves than did the wild type (9 versus 13) (Figure 4d). Rosette leaves of *atphb3^KO* plants were often curled and inflorescence growth was decreased. These growth-related phenotypes were complemented by *AtPHB3* expression because introduction of a Pro35S:AtPHB3 construct restored their growth rate (see below). *Atphb4^KO* (GABI_535 G10) had a T-DNA insertion in the second exon of *AtPHB4* (Figure 4a) and RNA gel blot analysis consolidated the absence of *AtPHB4* transcript in homozygous plants (Figure 4b). The *atphb4^KO* plants had no aberrant phenotypes compared with wild-type plants (data not shown).

The lack of a phenotype in *atphb4^KO* is probably due to a functional redundancy with *AtPHB3* that is expressed at higher levels (Figures 2a and 3b). Accordingly, in *atphb4^KO*, protein levels of type-I PHBs had not decreased compared with those of wild-type plants on protein gel blots with an antibody that recognizes type-I AtPHBs (Snedden and Fromm, 1997), while in *atphb3^KO* a drastic reduction in protein levels was observed (Figure 4b).

atphb3^KO plants have reduced growth rates

The significant developmentally related defects of *atphb3^KO* plants prompted us to investigate the effects of the *atphb3* mutation on growth rates at the cellular level. Therefore, we monitored the growth characteristics of the cortex cells in the root apical meristem. These cells are well suited to a kinematic growth analysis because they provide a linear model to study plant cell division and expansion rates (Beemster and Baskin, 1998; Fiorani and Beemster, 2006). Table 2 presents the average root cortex cell growth parameters of *atphb3^KO* and Col-0 plants 1 week after germination. The overall rate of root growth in wild-type plants
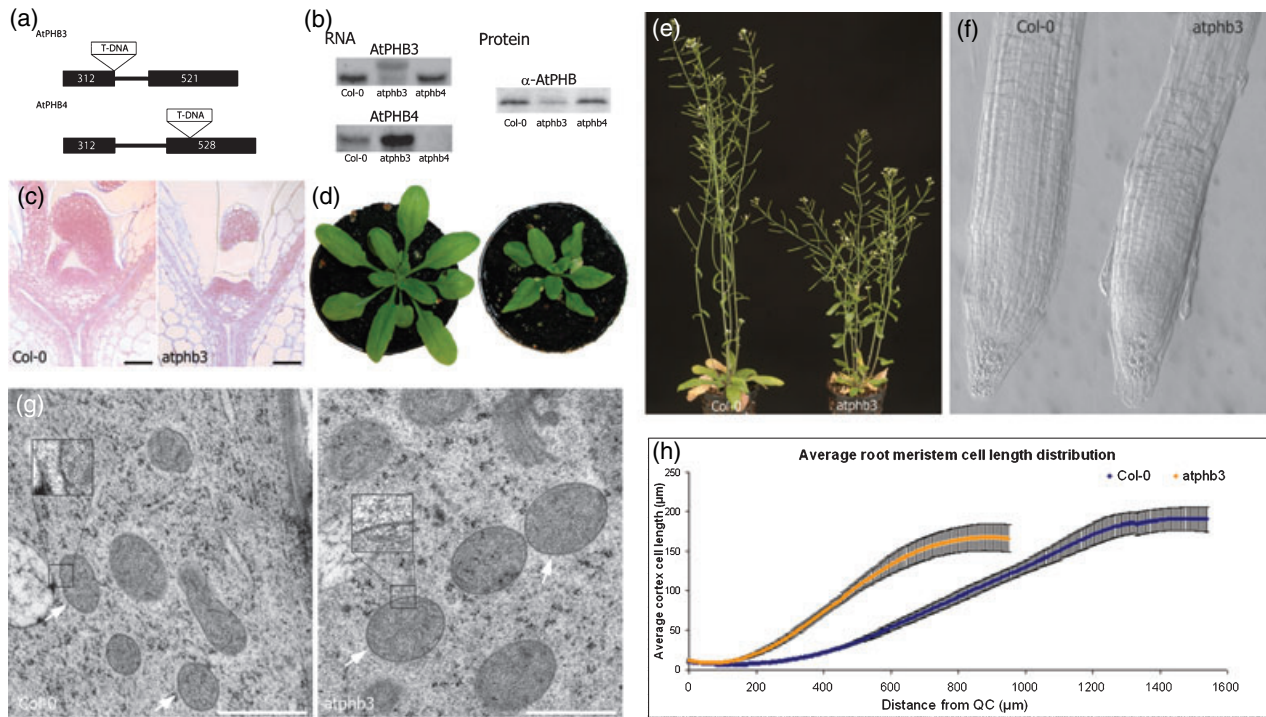
Figure 4. Characterization of an *atphb3* mutant of prohibitin (PHB).
(a) Position of T-DNA insertions in *atphb3*[KO] and *atphb4*[KO] mutants. Numbers indicate exon lengths in base pairs.
(b) RNA hybridizations with *AtPHB3* and *AtPHB4* probes on Col-0, *atphb3*[KO] and *atphb4*[KO] total RNA. Protein hybridization with anti-AtPHB3/4 antibody (Snedden and Fromm, 1997) on Col-0, *atphb3*[KO] and *atphb4*[KO] protein extracts (the band size is 30–31 kDa).
(c) Sections through the shoot apex of Col-0 and *atphb3*[KO] seedlings 3 days after stratification. Scale bars = 10 μm.
(d) Rosette shape of Col-0 and *atphb3*[KO] plants of the same age, just prior to bolting.
(e) Growth habit of mature Col-0 and *atphb3*[KO] plants.
(f) Differential interference contrast microscopy image of Col-0 and *atphb3*[KO] primary root tip.
(g) Transmission electron micrographs of Col-0 and *atphb3*[KO] columella cells. Arrows indicate mitochondria. Note the smoother membrane surface of *atphb3*[KO] mitochondria compared with wild-type mitochondria. Insets are a 2.5× magnification. Scale bars = 500 nm.
(h) Cell length distribution of Col-0 and *atphb3*[KO] root cortex cells and average distribution. A clear reduction in *atphb3*[KO] meristem size was observed, while mature cell length was not significantly altered. Error bars give SE. QC, quiescent center.

Parameter	Col-0	*atphb3*[KO]	*atphb3*[KO]/Col-0 ratio	*P*-value
Root elongation rate (μm h^{-1})	297 ± 8	80 ± 4	0.27	0.0001
Growth zone size (μm)	1242 ± 72	773 ± 50	0.62	0.0001
Mature cell length (μm)	180 ± 12	166 ± 9	0.92	n.s.
Meristem size (μm)	528 ± 15	334 ± 16	0.63	0.0001
Meristem cell number	55 ± 1	25 ± 2	0.45	0.0001
Cell cycle duration (h)	23.3 ± 1.7	35.3 ± 2.7	1.51	0.0029
Cell production rate (cells h^{-1})	1.70 ± 0.13	0.49 ± 0.02	0.29	0.0001
Time in division zone (h)	135 ± 10	164 ± 17	1.21	n.s.
Time in elongation zone (h)	5 ± 1	10 ± 1	2.07	0.0004
Elongation zone cell number	8 ± 1	5 ± 1	0.61	0.0015
Expansion rate (% h^{-1})	29.1 ± 2.7	13.2 ± 0.6	0.45	0.0007

Table 2 Overview of growth parameters of wild-type and *atphb3*[KO] cortex cells in the root apical meristem

n.s., not significant.

was approximately 300 μm h^{-1}, whereas in *atphb3*[KO] roots it was less than 100 μm h^{-1}. Despite a reduction in cellular diameter (123 ± 4 μm in *atphb3*[KO] versus 145 ± 5 μm in Col-0; *P* < 0.0001), the diminished growth rate was not due to a significant decrease in the length of mature cells, but rather to a decrease in production of meristem cells and the rate of cell expansion. The size of the root meristem was reduced from 528 ± 15 μm in Col-0 to 334 ± 16 μm in *atphb3*[KO] (Figure 4h). Furthermore, the number of cells in the *atphb3*[KO] root meristem was more than two-fold lower than

that in wild-type plants and the average duration of cell division was significantly increased from 23.3 ± 1.7 h (Col-0) to 35.3 ± 2.7 h (*atphb3^{KO}*). As a result, the *atphb3^{KO}* root meristem produced only 0.49 ± 0.02 cells h^{-1}, as opposed to 1.7 ± 0.13 cells h^{-1} for the wild type. Besides the cell division rate, cell expansion was also influenced. Root meristem cells spend most of their growth in the division (meristematic) zone (135 ± 10 h in Col-0; Table 2), and once they leave the actual meristem they expand very rapidly to their mature size in a matter of hours (5 ± 1 h in Col-0). In a wild-type root tip, approximately eight cells were in the expansion phase compared with only five in *atphb3^{KO}*. Moreover, the rate of cell expansion itself in *atphb3^{KO}* roots was less than half of that in wild-type roots. This loss was largely compensated in *atphb3^{KO}* roots by allowing the cells to spend twice as long in the expansion phase (5 ± 1 h for Col-0 versus 10 ± 1 h in *atphb3*), so in the end the cells could reach a normal mature cell length. In conclusion, *AtPHB3* is required to support proficient cell division and expansion rates in growing plant tissues.

atphb3^{KO} *plants display an aberrant mitochondrial morphology*

The root tips of wild-type and *atphb3^{KO}* seedlings were examined by transmission electron microscopy (Figure 4g). A striking difference in *atphb3^{KO}* sections was the presence of large-sized mitochondria. To quantify this difference, we measured the section plane of mitochondria in multiple sections. A more than two-fold increase in the section plane was noticed [0.076 ± 0.003 μm^2 ($n = 104$) versus 0.163 ± 0.005 μm^2 ($n = 92$) in wild type versus *atphb3^{KO}*]. Qualitatively, *atphb3^{KO}* mitochondria had a rounder, egg-like morphology together with a smoother surface than those of the more ruffled wild-type mitochondrial membranes (Figure 4g).

Type-I AtPHBs are interchangeable for growth proficiency

By crossing *atphb3^{KO}* and *atphb4^{KO}* T-DNA insertion lines, we attempted to generate *atphb3^{KO} atphb4^{KO}* plants. However, within the F$_2$ progeny no plants homozygous for the two T-DNA insertions could be found with PCR-based genotyping ($n = 120$) nor homozygous for one insertion and hemizygous for the other. To further address the functional redundancy between the type-I *AtPHB* genes, we tested whether the *atphb3^{KO}* growth retardation phenotype could be complemented by the introduction of *AtPHB3* or *AtPHB4*. Therefore, *atphb3^{KO}* plants were transformed with a Pro35S:AtPHB3 and Pro35S:AtPHB4 construct, respectively. Transformants were selected and homozygous lines were produced. In both complementations, germination and root elongation rates were restored (Supplementary Figure S1), indicating that type-I PHBs are exchangeable for their role in

supporting meristem activities. Taken together, these complementation experiments and the inability to retrieve a double mutant indicate that an undefined threshold level of type-I AtPHB is necessary to obtain viable plantlets and to support proficient meristematic activities. *AtPHB3* appears to be the predominant type-I *AtPHB* acting in the mitochondria, because these threshold levels are jeopardized by loss of function of *AtPHB3* and not *AtPHB4* and total type-I AtPHB protein levels are appreciably reduced only in *atphb3^{KO}* plants (Figure 4b). We also transformed *atphb3^{KO}* plants with Pro35S-driven expression constructs containing the type-II *AtPHB1*, *AtPHB2* and *AtPHB6*. None of the transformants had root growth or germination speed restored, indicative of a distinct functionality of the type-II PHBs (Supplementary Figure S1).

Overproduction of type-I AtPHBs affects plant architecture

Transgenic lines overproducing type-I AtPHBs were produced by transforming Arabidopsis with Pro35S:AtPHB3 and Pro35S:AtPHB4 constructs. Independent transformants with single-locus transgene insertions were retained for further analysis. Increased levels of *AtPHB* genes in the selected lines were confirmed by RNA and protein blot analyses (Figure 5c). Ectopic expression of *AtPHB3* and *AtPHB4* did not lead to aberrant phenotypes early in development and root growth rates were identical to those of wild-type plants (data not shown). However, at later developmental stages, both *AtPHB3^{OE}* and *AtPHB4^{OE}* had irregularly shaped leaves and, after emergence of the inflorescence, increased shoot branching (Figure 5a,b,d,e). In *AtPHB3^{OE}* plants, the irregular rosette shapes were most apparent, leading to a reduction in biomass, while shoot branching was most prominent in *AtPHB4^{OE}* plants. Occasionally, inflorescence fasciations were noted. Overexpressing lines had a shorter stature than wild-type plants (Figure 5a,b,d).

AtPHB perturbation provokes the accumulation of stress-related transcripts

To obtain further insights into the downstream effects provoked by *AtPHB3* and *AtPHB4* perturbations, we used gene expression data as a molecular phenotype. Wild-type, *atphb3^{KO}*, *atphb4^{KO}*, Pro35S:AtPHB3 (*AtPHB3^{OE}*) and Pro35S:AtPHB4 (*AtPHB4^{OE}*) plants were analyzed by genome-wide microarrays. Transcriptomes of the different transgenic lines were compared at developmental stage 1.04 (Boyes *et al.*, 2001). Except for the growth retardation of *atphb3^{KO}* seedlings (Figure 4), no phenotypical differences were detectable between wild-type and transgenic plants at this stage. Three independent samples per genotype of pooled seedlings grown *in vitro* were harvested; RNA was prepared and hybridized to full-genome Affymetrix ATH1 Genechip microarrays. Probe sets with a fold change greater
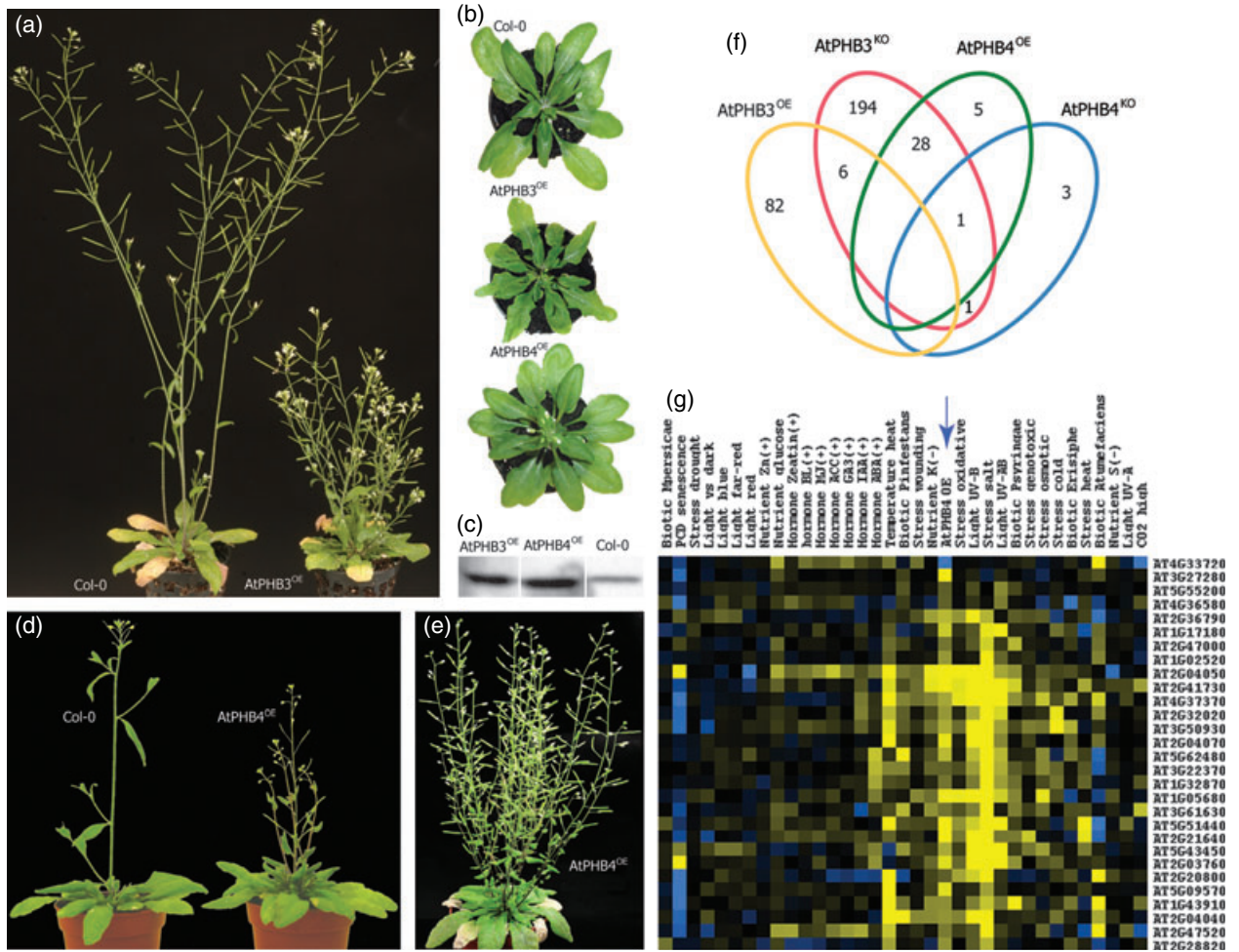
Figure 5. Type-I *AtPHB* overexpression plants and microarray analysis.
(a) Growth habit of mature Col-0 and *AtPHB3*[OE] plants.
(b) Rosette shapes of Col-0, *AtPHB3*[OE] and *AtPHB4*[OE] plants.
(c) Protein hybridizations with an anti-prohibitin (PHB) antibody on Col-0, *AtPHB3*[OE] and *AtPHB4*[OE] plants.
(d) Growth habit of Col-0 and *AtPHB4*[OE] plants early in bolting.
(e) Growth habit of a mature *AtPHB4*[OE] plant.
(f) Venn diagram representation of microarray experiments performed on type-I *AtPHB* perturbation lines (numbers indicate differential probe sets).
(g) Hierarchical average linkage clustering of *AtPHB4*[OE]/*atphb3*[KO]-regulated genes from publicly available microarray experiments. Blue, downregulation; yellow, upregulation; black, no change.

than 2 ($P < 0.05$ after multiple testing correction) were considered as differentially expressed. The complete inventory of differential probe sets can be found in Supplementary Table S1. Reproducibility of the ATH1 microarray hybridizations was assessed by monitoring the expression of a representative set of genes by real-time RT-PCR on biological replicate experiments (data not shown).

In the *atphb3*[KO] seedlings, 130 and 100 probe sets were upregulated and downregulated, respectively. A strong effect of the *atphb3*[KO] mutation on mitochondrial metabolism – as noted earlier by aberrant mitochondrial phenotypes (Figure 4g) – was also reflected at the transcriptional level. Of the differentially expressed probe sets, 38 were known or predicted to be imported in the mitochondria [the Arabidopsis Subcellular Database (SUBA)], of which seven

were involved in oxidative phosphorylation. Other upregulated probe sets included genes associated with transport and glycolysis. Several genes involved in cell wall metabolism and disease resistance were downregulated in *atphb3*[KO] seedlings. A breakdown into functional categories of the differential probe sets in *atphb3*[KO] seedlings can be found in Supplementary Table S1. Transcriptional changes in *atphb4*[KO] plants were minor: only one probe set was upregulated and three were downregulated (including *AtPHB4*). A high-affinity nitrate transporter was detected in the upregulated probe set, which was also upregulated in *atphb3*[KO] plants. *MPK12* and an expressed protein (At2g46080) were downregulated. In *AtPHB3*[OE] seedlings, 27 probe sets were upregulated and 61 were downregulated. Six genes involved in disease resistance were upregulated

Table 3 Genes differential (>2-fold change, $P < 0.05$) in both *atphb3*[KO] and *AtPHB4*[OE] lines as determined by ATH1 microarray analysis. The numbers indicate fold change values relative to Col-0 wild type

Probe set	AGI code	Description	AtPHB4[OE]	atphb3[KO]
257149_at	At3g27280	*AtPHB4* prohibitin	30.17	2.29
263515_at	At2g21640	Expressed mitochondrial protein	10.96	45.07
263402_at	At2g04050	MATE efflux family protein	10.38	31.49
260522_x_at	At2g41730	Expressed mitochondrial protein	10.21	28.88
248434_at	At5g51440	23.5 kDa mitochondrial heat shock protein	7.43	15.50
263231_at	At1g05680	UDP-glucosyltransferase *UGT74E2*	6.32	6.88
263401_at	At2g04070	MATE efflux family protein	5.78	5.15
264042_at	At2g03760	Steroid sulfotransferase *AtST1*	5.34	9.26
250515_at	At5g09570	Expressed protein	5.32	31.67
262517_at	At1g17180	Glutathione-*S*-transferase	4.64	4.91
247435_at	At5g62480	Putative glutathione-*S*-transferase	4.03	3.93
265200_s_at	At2g36790	UDP-glucosyltransferase *UGT73C6*	3.99	6.29
252131_at	At3g50930	*BCS1* mitochondrial AAA-type ATPase	3.59	4.28
249125_at	At5g43450	2-oxoglutarate-dependent dioxygenase	3.56	5.02
253046_at	At4g37370	Cytochrome P450 *CYP81D8*	3.49	5.31
260932_s_at	At1g02520	*PGP11* ABC transporter	3.1	3.11
265668_at	At2g32020	GCN5-related *N*-acetyltransferase	3.08	4.51
263403_at	At2g04040	MATE efflux family protein	3.02	4.65
266217_at	At2g28820	Ribosomal protein L16	2.99	19.19
259507_at	At1g43910	AAA-type ATPase	2.9	2.62
245173_at	At2g47520	Putative AP2 transcription factor	2.51	5.56
266752_at	At2g47000	*PGP4* ABC auxin-transporter	2.39	3.33
261192_at	At1g32870	No apical meristem (NAM) protein	2.38	6.21
251282_at	At3g61630	AP2 transcription factor *CRF6*	2.38	5.32
258452_at	At3g22370	Alternative oxidase 1a *Aox1a*	2.07	5.01
246282_at	At4g36580	AAA-type ATPase	2.05	4.01
265422_at	At2g20800	Alternative NADH-dehydrogenase *NDB4*	2.04	12.80
248101_at	At5g55200	Co-chaperone grpE protein	2.03	3.43
253301_at	At4g33720	Pathogenesis-related similar to PR-1	0.1	0.40

MATE, multidrug and toxin extrusion; AAA, [matrix-ATPases] associated with a variety of activities; ABC, ATP-binding cassette; UDP, uridine 5′-diphosphate.

and 15 genes predicted or annotated to be imported into the chloroplasts were downregulated. In *AtPHB4*[OE] seedlings, 32 probe sets were upregulated and 2 were downregulated. Remarkably, comparison of the differentially expressed probe sets from all four configurations revealed that 29 out of 34 probe sets up- or downregulated in *AtPHB4*[OE] lines had similar expression characteristics in *atphb3*[KO] plants (Figure 5f and Table 3).

With the Genevestigator toolbox, the expression pattern of the 29 *AtPHB4*[OE]/*atphb3*[KO]-specific probe sets was assessed in more than 2000 publicly available microarray experiments (Zimmermann *et al.*, 2004). Most of these genes were significantly upregulated under several abiotic stress conditions, mainly salt, UV-B, heat and oxidative stress (Figure 5g). In addition, a Spearman correlation analysis on the microarray data sets from the publicly available AtGenExpress time course experiments of cold, osmotic, salt, oxidative and UV-B stress (160 ATH1 chips; http://www.arabidopsis.org) indicates that these *AtPHB4*[OE]/*atphb3*[KO]-specific probe sets are co-regulated during abiotic stress conditions (Supplementary Table S2). Remarkably, a set of at least five genes had very high mutual correlation

coefficients and was thus strongly co-expressed: *At2g04050* (MATE efflux carrier), *At2g41730* (expressed mitochondrial protein), *At1g05680* (UGT74E2), *At4g37370* (cytochrome P450 CYP81D8) and *At2g04040* (MATE efflux carrier).

Discussion

AtPHBs form a multimeric mitochondrial complex

We have demonstrated that in Arabidopsis at least five PHBs are expressed and targeted to the mitochondria. A TAP-based interaction study showed that type-I and type-II AtPHBs are found together in a multimeric complex. In fungi and metazoans, PHB1 and PHB2 form a ring-shaped complex of 1–2 MDa in the inner mitochondrial membrane (Tatsuta *et al.*, 2005). In Arabidopsis, Blue Native-PAGE experiments indicated that PHBs are present in the largest (>1 MDa) detectable mitochondrial complex (Heazlewood *et al.*, 2003). Although PHBs have previously been suggested to interact with m-AAA proteases and to act as chaperones for respiratory chain components (Nijtmans *et al.*, 2000; Steglich *et al.*, 1999), no interacting proteins

were found in the TAP complexes that support this hypothesis. The interaction with a mitochondrial citric acid cycle enzyme (isocitrate dehydrogenase IDH1) and the glycolytic enzyme phosphoglycerate kinase, previously shown to be associated with plant mitochondria (Giegé *et al.*, 2003) suggests an interplay of AtPHBs with ATP/energy production. Alternatively, the AtPHB complex might play a role in channeling metabolites by forming pores in the mitochondrial membrane (Nadimpalli *et al.*, 2000) and the upregulation of respiratory and glycolytic enzymes in the *atphb3*[KO] plants (Supplementary Table S1) might reflect a cellular attempt to restore perturbed energy metabolism in these loss-of-function mutants.

Type-I AtPHBs are required for proficient growth rates in apical tissues

High AtPHB levels in proliferative tissues, such as the leaf primordia, the root apical meristem and lateral root initials, are in contrast to a previously suggested negative correlation of *AtPHB4* mRNA levels and root growth rate (de Diego *et al.*, 2007). That normal root and shoot apex development is disturbed in plants in which the most abundantly expressed type-I *AtPHB3* is lost supports an important function of type-I AtPHBs within dividing plant tissues. Previously, RNA interference experiments suggested that PHBs are also important in proliferating reproductive tissues of *C. elegans* (Artal-Sanz *et al.*, 2003).

The reduced meristematic activity, increased duration of cell division and decreased cell elongation rates, together impair tissue growth. The increased shoot branching and sporadically observed inflorescence fasciations in type-I *AtPHB*[OE] lines also hint at a disturbed meristem organization and/or proliferative status. How *AtPHB* genes influence meristematic activities might be explained by taking into account the role of PHBs in mitochondrial biogenesis, maintenance and/or function in these rapidly dividing and developing tissues in which new functional mitochondria need to be constructed. Alternatively, elevated levels of AtPHBs in the mitochondria might facilitate the increased energy metabolism needed to support intensive rates of cell division in meristematic tissues, because actively dividing cells depend on high ATP production to allow energy-demanding processes such as DNA replication and cytokinesis (Elorza *et al.*, 2004).

The effect of the *atphb3*[KO] mutation on mitochondrial homeostasis is also supported by the molecular phenotype of *atphb3*[KO] plants. Within the set of differentially expressed genes, almost 40 are annotated as or experimentally demonstrated to be located in the mitochondria. This set includes genes involved in respiration: alternative NADH-dehydrogenases (NDB3 and NDB4), alternative oxidases Aox1a and Aox1c, cytochrome *b* and proteins involved in assembly of Complex III and IV (BCS1 and an SCO-related protein). Also

several transcripts encoding proteins functioning in mitochondrial transport and protein folding are upregulated. Besides mitochondrial energy metabolism, glycolytic enzymes were differentially expressed: a pyruvate kinase, fructose bisphosphate aldolase and phosphoglycerate mutase were upregulated and another pyruvate kinase was downregulated. Two enzymes involved in biosynthesis of the pyruvate kinase co-factor thiamine and of riboflavin, the precursor of FAD and flavine mononucleotide (FMN), both co-factors in the respiration chain, were upregulated. On the other hand, many genes involved generally in electron transport were downregulated: CYP450s, peroxidases and FAD-binding proteins, possibly reflecting an altered redox state of *atphb3*[KO] cells.

Prohibitins have been reported to act as anti-proliferative tumor-suppressor genes in mammalian cell cultures, hence the name 'prohibitin' (Nuell *et al.*, 1991; Wang *et al.*, 1999). However, a positive role for Arabidopsis mitochondrial PHBs in dividing tissues is more in line with the high levels of mammalian PHBs in primary human tumors and the direct transcriptional control of mammalian *PHB* genes by c-Myc, a major transcription factor promoting cell division that is often activated during oncogenesis (Coates *et al.*, 2001; Menssen and Hermeking, 2002). In plants, PHBs would probably not act as anti-proliferative proteins because, in contrast to mammalian PHBs, AtPHBs do not interact with key nuclear cell cycle components such as E2F and retinoblastoma-related proteins (O.V.A. and F.V.B. unpublished data; de Diego *et al.*, 2007).

PHB and mitochondrial retrograde signaling?

Microarray analysis of both *AtPHB3* and *AtPHB4* loss-of-function and overexpression lines revealed an overlapping set of 29 transcripts with increased levels in both *AT-PHB4*[OE] and *atphb3*[KO] plants, the latter with elevated levels of *AtPHB4*. Through a microarray meta-analysis we showed that the abundance of these transcripts changed under specific abiotic stress conditions, such as salt, UV-B, oxidative and heat stress. Besides mitochondrial genes (*HSP23.5*, *BCS1*, *Aox1a*, *NDB4*, a grpE co-chaperone and three unknown mitochondrial proteins), this gene set includes several genes involved in transport and modification [three multidrug and toxin extrusion (MATE) efflux carriers, two ATP-binding cassette (ABC) transporters, two glutathione-*S*-transferases, two glucosyltransferases, a cytochrome P450 and a steroid sulfotransferase] together with four transcription factors. The relationship of this gene set with mitochondrial homeostasis is further corroborated by an independent microarray meta-analysis showing that five of the genes (*At1g32870*, NAM transcription factor; *At2g41730*, expressed mitochondrial protein; *At4g37370*, CYP81D8; *At2g03760*, steroid sulfotransferase *AtST1*; and *At1g05680*, *UGT74E2*) are highly co-regulated with

Aox1a (a gene known to be regulated by mitochondrial retrograde signaling) during stress (Expression Angler; Toufighi *et al.*, 2005; Dojcinovic *et al.*, 2005). Five more genes were among the top 50 (*At3g61630*, AP2 transcription factor; *At5g43450*, 2-oxoglutarate dioxygenase; *At2g04050*, MATE efflux carrier; *At2g32020*, GNAT family protein; *At2g04070*, MATE efflux carrier). The changes in abundance of stress-related genes caused by imbalances in the synthesis of AtPHBs indicate how important AtPHBs are for mitochondrial function, although AtPHBs themselves are not necessarily directly involved in upregulation of these genes. Which mitochondrial signals are produced by the perturbation of AtPHB and how they impinge on nuclear gene expression remains elusive at this stage.

Experimental procedures

Sequence analysis

The PHB protein sequences of representative organisms were collected from the non-redundant GenBank protein database and the *Populus trichocarpa* PHBs from http://genome.jgi-psf.org/Poptr1/Poptr1.home.html. The sequences were aligned with CLUSTALW (Thompson *et al.*, 1994) and a phylogenetic tree was generated with Treecon (Van de Peer and De Wachter, 1994) with 1000 bootstrap trials. To assess the subcellular localization of the seven AtPHBs based on the amino acid sequences, various prediction software tools available on the World Wide Web were used (Psort, TargetP, MitoProt, Predotar, Softberry and TMHMM2). Genomic sequences for the AtPHBs were collected from http://www.arabidopsis.org.

Cloning of Arabidopsis open reading frames

Open reading frames were amplified by PCR from first-strand cDNA of *A. thaliana* (L). Heynh. ecotype Columbia (Col-0). The forward and reverse primers are given in Supplementary Table S3. In a second PCR round, the amplicons were extended with the attB1 and attB2 primers. All products were cloned into pDONR221 (Invitrogen, http://www.invitrogen.com/).

Subcellular localization

The *AtPHB* ORFs were recombinationally cloned from pDONR221 into the binary vectors pK7FWG2 and pK7WGF2 (Karimi *et al.*, 2002). These constructs were transformed into *N. tabacum* BY-2 cell suspensions as described (Vanstraelen *et al.*, 2004). Transformed calli were selected and analyzed with a confocal microscope, consisting of an inverted Axiovert 100 M (Zeiss, http://www.zeiss.com/), equipped with a 63× water-corrected objective (numerical aperture 1.2) and an argon ion laser. Mitotracker Red (Molecular Probes; http://www.probes.invitrogen.com) was used as mitochondrial marker for co-localization.

Plant material, growth conditions and transformation

Arabidopsis Col-0 seeds were sterilized by overnight incubation with chlorine gas (100 ml 12% NaOCl and 3 ml 37% HCl). Plants were grown on 4.3 g l^{-1} MS medium (Duchefa, http://www.duchefa.com/), 0.5 g l^{-1} 2-(*N*-morpholino)ethanesulfonic acid, 0.1 g l^{-1} myo-inositol, 20 g l^{-1} sucrose, 7 g l^{-1} plant tissue culture agar (LabM, http://www.labm.com/), 0.5 mg l^{-1} nicotinic acid, 0.5 mg l^{-1} pyridoxine and 1 mg l^{-1} thiamine) at 21°C and 65 µE m^{-2} sec^{-1} radiation in a 16-h light/8-h dark photoperiod. Arabidopsis plants were transformed with the *A. tumefaciens*-mediated floral dip (Clough and Bent, 1998). Transformants with the *bar* resistance gene were selected by spraying with 40 mg l^{-1} Pestanal (glufosinate ammonium; Sigma-Aldrich, http://www.sigmaaldrich.com/) or on MS medium containing 5 mg l^{-1} glufosinate ammonium. Transformant lines with a single T-DNA locus were selected by segregation analysis.

Tandem affinity purification

Tandem affinity purification experiments were carried out according to Van Leene *et al.* (2007). In short, the AtPHB3-coding sequence was cloned by recombination into the pKCTAP vector generating a Pro35S:*AtPHB3*-TAP cassette (pKCATPHB3TAP). Arabidopsis cell suspension cultures were stably transformed by *A. tumefaciens*-mediated co-cultivation with pKCATPHB3TAP. Transformed Arabidopsis cells were selected and transferred to liquid medium for upscaling. Expression levels of TAP-tagged proteins were checked by protein blotting with an anti-CBP antibody (data not shown). In a first round of affinity purification, protein extracts of 15 g of plant material were incubated with an IgG resin. Bound complexes were released and eluted from the resin by tag cleavage with TEV protease. In a second affinity step on a calmodulin agarose column, co-eluting non-interacting proteins and the TEV protease were removed with the flow-through. Finally, both the AtPHB3 bait and interacting proteins were eluted from the calmodulin agarose via EGTA-mediated removal of calcium. Eluted proteins were separated on 4–12% NuPAGE gels, excised and analyzed by MS. To increase the stringency of the data set, contaminating proteins because of experimental background as determined by Van Leene *et al.* (2007) were systematically subtracted from the lists of co-purified proteins. Most contaminants were highly abundant proteins, such as chaperones, cytoskeleton proteins, ribosomal proteins, metabolic enzymes or protein translation factors.

Generation of Arabidopsis overexpression lines

AtPHB genes were cloned by recombination from pDONR221 to the p35S overexpression vector pB7WG2 (Karimi *et al.*, 2002) and transformed into Arabidopsis Col-0. Overexpression of *AtPHB3* and *AtPHB4* was confirmed by RNA gel blotting with digoxigenin-labeled *AtPHB3* or *AtPHB4* full-length cDNA (Roche Diagnostics, http://www.roche.com/), by real-time PCR on an iCycler (Bio-Rad, http://www.bio-rad.com/) with a Real-Time PCR kit with SYBR-green (Invitrogen) and by protein gel blotting as described (Snedden and Fromm, 1997). Overexpression of the other genes was also confirmed by real-time RT-PCR. Actin-related protein 7 (At3g60830) was used as a housekeeping gene with Universal ProbeLibrary probe no. 147 (Roche Diagnostics). Primer sequences can be found in Supplementary Table S3.

Isolation of AtPHB3 and AtPHB4 insertion mutant lines

Homozygote plants from the GABI-Kat line (Rosso *et al.*, 2003) GABI_535 G10 with a T-DNA insertion into the second exon of *AtPHB4* were selected by PCR with primer sequences generated

against the genomic regions flanking the insert and a standard primer for the 3′ end of the insertion sequence, to obtain homozygous insertion lines (for primers, see Supplementary Table S3; Rosso *et al.*, 2003). The SALK lines SALK_020707 with an insertion in the *AtPHB3*-coding region were ordered from the Arabidopsis Biological Resource Center and screened by PCR for homozygous lines (for primers, see Supplementary Table S3).

Promoter-GUS analysis

The upstream *AtPHB* promoter region, the first exon, the first intron and approximately 20 bp of the second exon were amplified by PCR from Arabidopsis Col-0 genomic DNA (Supplementary Table S3). All PCR products were cloned into pBGWSF7 (Karimi *et al.*, 2002), generating an in-frame GFP-GUS fusion. All constructs were transformed into Arabidopsis Col-0 and assayed for GUS staining (Beeckman and Engler, 1994). Samples were photographed with a stereomicroscope (Stemi SV11; Zeiss) or with a differential interference contrast microscope (Leica, http://www.leica.com/). For the lateral root induction assay, supplements consisted of 10 μM NPA (Duchefa) or 10 μm NAA (Sigma-Aldrich).

Microarray analysis

Arabidopsis Col-0 and homozygous *AtPHB3*[OE], *AtPHB4*[OE], *atphb3*[KO] and *atphb4*[KO] seeds were sown on half-strength MS plant medium in triplicate. Per triplicate, the plantlets were harvested at developmental stage 1.04 (Boyes *et al.*, 2001). Total RNA was isolated with TRIzol reagent (Invitrogen). Each triplicate of Arabidopsis Col-0 and homozygous transgenic plants was hybridized to one Affymetrix chip (GeneChip®, Arabidopsis ATH1 Genome Array; Affymetrix, http://www.affymetrix.com). For each hybridization, 5 μg of total RNA was used and analyzed with Affymetrix chips at the VIB Microarray Facility (Leuven, Belgium) under the manufacturer's conditions (http://https://www.affymetrix.com). Raw data were processed in the BIOCONDUCTOR software package (Gentleman *et al.*, 2004) with the statistical algorithm robust multichip average (RMA; Irizarry *et al.*, 2003). The expression values were analyzed with the *limma* bioconductor package (Smyth, 2004) and a false discovery rate correction for multiple testing was applied (Benjamini and Hochberg, 1995). Genes with a differential regulation of at least twofold and a *P*-value smaller than 0.05 were selected.

Real-time RT-PCR analyses

For the housekeeping gene, the methods were as described above, whereas for At2g21640, At2g04050 and At2g41730 a real-time PCR kit with SYBR-green was used (for primers and probes, see Supplementary Table S3).

Data obtained from Genevestigator and correlation analysis

With the 'Response Viewer' tool of Genevestigator, the expression profiles of genes to different stimuli were analyzed (Zimmermann *et al.*, 2004). Tissue-specific expression values were examined with the 'Gene Atlas' tool. For more information on the described experiments, see http://https://www.genevestigator.ethz.ch. $\log_2$-transformed fold-change values were hierarchically clustered for genes and experiments by average linkage in GeneCluster (eisen@genome.stanford.edu). For the correlation analysis, the publicly available Affymetrix data from AtGenExpress (http://www.arabidopsis.org) on control versus cold, osmotic, salt (Kudla's

laboratory), oxidative (Bartels' laboratory) and UV-B (Harter's laboratory) stresses (160 ATH1 chips) were normalized with RMA and replicates were averaged. For each of the 34 differentially expressed probe sets in *AtPHB4*[OE] plants, the Spearman rank correlation coefficients with all 22 810 ATH1 probe sets were calculated (R statistical computing environment; http://www.r-project.org; Smyth, 2004). Probe sets were assigned ranks based on decreasing correlation coefficients.

Kinematic analysis

Wild-type and *atphb3*[KO] seeds were grown *in vitro* on vertical MS plates for 1 week. After full germination, root lengths were marked daily, the average root growth rates measured with the IMAGEJ software suite and the root tips photographed under a differential interference contrast microscope after 1 week. Images were stitched with the PANAVIEW software. Cell length profiles were made for seven wild-type and five transgenic roots and the different growth parameters were calculated according to Beemster *et al.* (2002).

Electron microscopy

Arabidopsis root tips were excised, briefly immersed in dextran 15–20% and frozen immediately in a high-pressure freezer (EM Pact, Leica Microsystems; http://www.leica-microsystems.com). Over a period of 4 days, tissues were freeze substituted in dry acetone containing 1% OsO_4 and 0.1% glutaraldehyde as follows: −90°C for 26 h, 2°C h^{-1} temperature increase over 15 h, −60°C for 8 h, 2°C h^{-1} temperature increase over 15 h, −30°C for 8 h with rinsing three times with acetone in a Leica EM Automatic Freeze Substitution. At the end, samples were slowly warmed up to 4°C and infiltrated at 4°C stepwise in Spurr's resin over 3 days. Ultrathin sections of gold interference color were cut with an ultramicrotome (ultracut E; Leica Microsystems) and collected on Formvar-coated copper slot grids. Sections were post-stained in an LKB ultrastainer (http://www.lkb.com.au/) for 40 min in uranyl acetate at 40°C and 10 min in lead stain at 20°C. Grids were viewed with a transmission electron microscope JEOL 1010 operating at 80 kV.

Supplementary Material

The following supplementary material is available for this article online:
Figure S1. Germination and root growth rate of *atphb3*[KO] complementations.
Table S1. Microarray analysis of type-I AtPHB perturbed lines.

Table S2. Spearman correlation analysis of AtPHB4^{OE}/atphb3^{KO}-induced genes.
Table S3. List of PCR primers and probes.
This material is available as part of the online article from http://www.blackwell-synergy.com

References

Ahn, C.S., Lee, J.H., Hwang, A.R., Kim, W.T. and Pai, H.-S. (2006) Prohibitin is involved in mitochondrial biogenesis in plants. *Plant J.* **46**, 658–667.

Artal-Sanz, M., Tsang, W.Y., Willems, E.M., Grivell, L.A., Lemire, B.D., van der Spek, H. and Nijtmans, L.G.J. (2003) The mitochondrial prohibitin complex is essential for embryonic viability and germline function in *Caenorhabditis elegans*. *J. Biol. Chem.* **278**, 32091–32099.

Beeckman, T. and Engler, G. (1994) An easy technique for the clearing of histochemically stained plant tissue. *Plant Mol. Biol. Rep.* **12**, 37–42.

Beemster, G.T.S. and Baskin, T.I. (1998) Analysis of cell division and elongation underlying the developmental acceleration of root growth in *Arabidopsis thaliana*. *Plant Physiol.* **116**, 1515–1526.

Beemster, G.T.S., De Vusser, K., De Tavernier, E., De Bock, K. and Inze, D. (2002) Variation in growth rate between Arabidopsis ecotypes is correlated with cell division and A-type cyclin-dependent kinase activity. *Plant Physiol*, **129**, 854–864.

Beemster, G.T.S., De Veylder, L., Vercruysse, S., West, G., Rombaut, D., Van Hummelen, P., Galichet, A., Gruissem, W., Inzé, D. and Vuylsteke, M. (2005) Genome-wide analysis of gene expression profiles associated with cell cycle transitions in growing organs of Arabidopsis. *Plant Physiol.* **138**, 734–743.

Benjamini, Y. and Hochberg, Y. (1995) Controlling the false discovery rate: a practical and powerful approach to multiple testing. *J. R. Stat. Soc. Ser. B.-Methodol.* **57**, 289–300.

Boyes, D.C., Zayed, A.M., Ascenzi, R., McCaskill, A.J., Hoffman, N.E., Davis, K.R. and Görlach, J. (2001) Growth stage-based phenotypic analysis of Arabidopsis: a model for high throughput functional genomics in plants. *Plant Cell*, **13**, 1499–1510.

Chen, J.-C., Jiang, C.-Z. and Reid, M.S. (2005) Silencing a prohibitin alters plant development and senescence. *Plant J.* **44**, 16–24.

Clough, S.J. and Bent, A.F. (1998) Floral dip: a simplified method for *Agrobacterium*-mediated transformation of *Arabidopsis thaliana*. *Plant J.* **16**, 735–743.

Coates, P.J., Jamieson, D.J., Smart, K., Prescott, A.R. and Hall, P.A. (1997) The prohibitin family of mitochondrial proteins regulate replicative lifespan. *Curr. Biol.* **7**, R607–R610.

Coates, P.J., Nenutil, R., McGregor, A., Picksley, S.M., Crouch, D.H., Hall, P.A. and Wright, E.G. (2001) Mammalian prohibitin proteins respond to mitochondrial stress and decrease during cellular senescence. *Exp. Cell Res.* **265**, 262–273.

de Diego, J.G., Rodríguez, F.D., Rodríguez Lorenzo, J.L. and Cervantes, E. (2007) The prohibitin genes in *Arabidopsis thaliana*: expression in seeds, hormonal regulation and possible role in cell cycle control during seed germination. *J. Plant Physiol.* **164**, 371–373.

Dojcinovic, D., Krosting, J., Harris, A.J., Wagner, D.J. and Rhoads, D.M. (2005) Identification of a region of the Arabidopsis *AtAOX1a* promoter necessary for mitochondrial retrograde regulation of expression. *Plant Mol. Biol.* **58**, 159–175.

Elorza, A., León, G., Gómez, I., Mouras, A., Holuigue, L., Araya, A. and Jordana, X. (2004) Nuclear *SDH2-1* and *SDH2-2* genes, encoding the iron-sulfur subunit of mitochondrial complex II in Arabidopsis, have distinct cell-specific expression patterns and promoter activities. *Plant Physiol.* **136**, 4072–4087.

Eloy, N.B., Coppens, F., Beemster, G.T.S., Hemerly, A.S. and Ferreira, P.C.G. (2006) The *Arabidopsis* anaphase promoting complex (APC): regulation through subunit availability in plant tissues. *Cell Cycle*, **5**, 1957–1965.

Fiorani, F. and Beemster, G.T.S. (2006) Quantitative analyses of cell division in plants. *Plant Mol. Biol.* **60**, 963–979.

Fusaro, G., Dasgupta, P., Rastogi, S., Joshi, B. and Chellappan, S. (2003) Prohibitin induces the transcriptional activity of p53 and is exported from the nucleus upon apoptotic signaling. *J. Biol. Chem.* **278**, 47853–47861.

Gamble, S.C., Odontiadis, M., Waxman, J., Westbrook, J.A., Dunn, M.J., Wait, R., Lam, E.W. and Bevan, C.L. (2004) Androgens target prohibitin to regulate proliferation of prostate cancer cells. *Oncogene*, **23**, 2996–3004.

Gentleman, R.C., Carey, V.J., Bates, D.M. *et al.* (2004) Bioconductor: open software development for computational biology and bioinformatics. *Genome Biol.* **5**, R80.1–R80.16.

Giegé, P., Heazlewood, J.L., Roessner-Tunali, U., Millar, A.H., Fernie, A.R., Leaver, C.J. and Sweetlove, L.J. (2003) Enzymes of glycolysis are functionally associated with the mitochondrion in Arabidopsis cells. *Plant Cell*, **15**, 2140–2151.

Heazlewood, J.L., Howell, K.A. and Millar, A.H. (2003) Mitochondrial complex I from Arabidopsis and rice: orthologs of mammalian and fungal components coupled with plant-specific subunits. *Biochim. Biophys. Acta*, **1604**, 159–169.

Himanen, K., Boucheron, E., Vanneste, S., de Almeida Engler, J., Inzé, D. and Beeckman, T. (2002) Auxin-mediated cell cycle activation during early lateral root initiation. *Plant Cell*, **14**, 2339–2351.

Ikonen, E., Fiedler, D., Parton, R.G. and Simons, K. (1995) Prohibitin, an antiproliferative protein, is localized to mitochondria. *FEBS Lett.* **358**, 273–277.

Irizarry, R.A., Hobbs, B., Collin, F., Beazer-Barclay, Y.D., Antonellis, K.J., Scherf, U. and Speed, T.P. (2003) Exploration, normalization, and summaries of high density oligonucleotide array probe level data. *Biostatistics*, **4**, 249–264.

Karimi, M., Inzé, D. and Depicker, A. (2002) GATEWAY™ vectors for *Agrobacterium*-mediated plant transformation. *Trends Plant Sci.* **7**, 193–195.

Krogh, A., Larsson, B., von Heijne, G. and Sonnhammer, E.L.L. (2001) Predicting transmembrane protein topology with a hidden Markov model: application to complete genomes. *J. Mol. Biol.* **305**, 567–580.

McClung, J.K., Danner, D.B., Stewart, D.A., Smith, J.R., Schneider, E.L., Lumpkin, C.K., Dell'Orco, R.T. and Nuell, M. (1989) Isolation of a cDNA that hybrid selects antiproliferative mRNA from rat liver. *Biochem. Biophys. Res. Commun.* **164**, 1316–1322.

Menssen, A. and Hermeking, H. (2002) Characterization of the c-MYC-regulated transcriptome by SAGE: identification and analysis of c-MYC target genes. *Proc. Natl Acad. Sci. USA*, **99**, 6274–6279.

Millar, A.H., Sweetlove, L.J., Giegé, P. and Leaver, C.J. (2001) Analysis of the Arabidopsis mitochondrial proteome. *Plant Physiol.* **127**, 1711–1727.

Mishra, S., Murphy, L.C., Nyomba, B.L.G. and Murphy, L.J. (2005) Prohibitin: a potential target for new therapeutics. *Trends Mol. Med.* **11**, 192–197.

Nadimpalli, R., Yalpani, N., Johal, G.S. and Simmons, C.R. (2000) Prohibitins, stomatins, and plant disease response genes compose a protein superfamily that controls cell proliferation, ion channel regulation, and death. *J. Biol. Chem.* **275**, 29579–29586.

Nijtmans, L.G.J., de Jong, L., Artal-Sanz, M.A., Coates, P.J., Berden, J.A., Back, J.W., Muijsers, A.O., van der Spek, H. and Grivell, L.A. (2000) Prohibitins act as a membrane-bound chaperone for the stabilization of mitochondrial proteins. *EMBO J.* **19**, 2444–2451.

Nuell, M.J., Stewart, D.A., Walker, L. *et al.* (1991) Prohibitin, an evolutionarily conserved intracellular protein that blocks DNA synthesis in normal fibroblasts and HeLa cells. *Mol. Cell. Biol.* **11**, 1372–1381.

Rajalingam, K., Wunder, C., Brinkmann, V., Churin, Y., Hekman, M., Sievers, C., Rapp, U.R. and Rudel, T. (2005) Prohibitin is required for Ras-induced Raf-MEK-ERK activation and epithelial cell migration. *Nat. Cell Biol.* **7**, 837–843.

Rigaut, G., Shevchenko, A., Rutz, B., Wilm, M., Mann, M. and Séraphin, B. (1999) A generic protein purification method for protein complex characterization and proteome exploration. *Nat. Biotechnol.* **17**, 1030–1032.

Rosso, M.G., Li, Y., Strizhov, N., Reiss, B., Dekker, K. and Weisshaar, B. (2003) An *Arabidopsis thaliana* T-DNA mutagenized population (GABI-Kat) for flanking sequence tag-based reverse genetics. *Plant Mol. Biol.* **53**, 247–259.

Smyth, G.K. (2004) Linear models and empirical Bayes methods for assessing differential expression in microarray experiments. *Stat. Appl. Genet. Mol. Biol.* **3**, No. 1. Article 3, 1–25 (http//http://www.bepress.com/sagmb/vol3/iss1/art3).

Snedden, W.A. and Fromm, H. (1997) Characterization of the plant homologue of prohibitin, a gene associated with antiproliferative activity in mammalian cells. *Plant Mol. Biol.* **33**, 753–756.

Steglich, G., Neupert, W. and Langer, T. (1999) Prohibitins regulate membrane protein degradation by the *m*-AAA protease in mitochondria. *Mol. Cell. Biol.* **19**, 3435–3442.

Tatsuta, T., Model, K. and Langer, T. (2005) Formation of membrane-bound ring complexes by prohibitins in mitochondria. *Mol. Biol. Cell*, **16**, 248–259.

Terashima, M., Kim, K.-M., Adachi, T., Nielsen, P.J., Reth, M., Köhler, G. and Lamers, M.C. (1994) The IgM antigen receptor of B lymphocytes is associated with prohibitin and a prohibitin-related protein. *EMBO J.* **13**, 3782–3792.

Thompson, J.D., Higgins, D.G. and Gibson, T.J. (1994) CLUSTAL W: improving the sensitivity of progressive multiple sequence alignment through sequence weighting, position-specific gap penalties and weight matrix choice. *Nucleic Acids Res.* **22**, 4673–4680.

Toufighi, K., Brady, S.M., Austin, R., Ly, E. and Provart, N.J. (2005) The Botany Array Resource: e-Northerns, Expression Angling, and promoter analyses. *Plant J.* **43**, 153–163.

Van de Peer, Y. and De Wachter, R. (1994) TREECON for Windows: a software package for the construction and drawing of evolutionary trees for the Microsoft Windows environment. *Comput. Appl. Biosci.* **10**, 569–570.

Van Leene, J., Eeckhout, D., Stals, H. *et al.* (2007) Tandem affinity purification of cell cycle protein complexes from *Arabidopsis* cell suspension cultures. *Mol. Cell. Proteomics*, **6**, 1226–1238.

Vanneste, S., De Rybel, B., Beemster, G.T.S. *et al.* (2005) Cell cycle progression in the pericycle is not sufficient for SOLITARY ROOT/IAA14-mediated lateral root initiation in *Arabidopsis thaliana*. *Plant Cell* **17**, 3035–3050.

Vanstraelen, M., Torres Acosta, J.A., De Veylder, L., Inzé, D. and Geelen, D. (2004) A plant-specific subclass of C-terminal kinesins contains a conserved A-type cyclin-dependent kinase site implicated in folding and dimerization. *Plant Physiol.* **135**, 1417–1429.

Wang, S., Nath, N., Adlam, M. and Chellappan, S. (1999) Prohibitin, a potential tumor suppressor, interacts with RB and regulates E2F function. *Oncogene*, **18**, 3501–3510.

Wang, S., Fusaro, G., Padmanabhan, J. and Chellappan, S.P. (2002) Prohibitin co-localizes with Rb in the nucleus and recruits N-CoR and HDAC1 for transcriptional repression. *Oncogene*, **21**, 8388–8396.

Zimmermann, P., Hirsch-Hoffmann, M., Hennig, L. and Gruissem, W. (2004) GENEVESTIGATOR. Arabidopsis microarray database and analysis toolbox. *Plant Physiol.* **136**, 2621–2632.